JOURNAL OF GUIDANCE, CONTROL, AND DYNAMICS
Vol. 19, No. 5, September–October 1996

# Gain-Scheduled Bank-to-Turn Autopilot Design Using Linear Parameter Varying Transformations

Lance H. Carter* and Jeff S. Shamma†
*University of Texas at Austin, Austin, Texas 78712-1085*

**A gain-scheduled autopilot design for a bank-to-turn missile is presented. The approach follows previous work for a longitudinal missile autopilot. The method is novel in that the gain-scheduled design does not involve linearizations about operating points. Instead, the missile dynamics are brought to a linear parameter varying form via a state transformation. A linear parameter varying system is defined as a linear system whose dynamics depend on an a priori unknown but measurable exogenous parameter. This framework is applied to the design of a coupled longitudinal/lateral bank-to-turn missile autopilot. The pitch and yaw/roll dynamics are separately transformed to linear parameter varying form, where the cross axis states are treated as exogenous parameters. These are actually endogenous variables, and so such a plant is called quasilinear parameter varying. Once in quasilinear parameter varying form, a family of robust controllers using $\mu$ synthesis is designed for both the pitch and yaw/roll channels, using angle of attack and roll rate as the scheduling variables. The closed-loop time response is simulated using the original nonlinear model and also using perturbed aerodynamic coefficients.**

## Nomenclature

| | |
|---|---|
| $C_l, C_m, C_n$ | = aerodynamic moment coefficients about body $x$, $y$, and $z$ axes |
| $C_x, C_y, C_z$ | = aerodynamic force coefficients along body $x$, $y$, and $z$ axes |
| $d$ | = reference diameter |
| $I_{xx}, I_{yy}, I_{zz}, I_{xz}$ | = moments of inertia |
| $I_1 - I_5$ | = constants dependent on moments of inertia (see Appendix) |
| $K_a$ | = actuator bandwidth, 188.5 rad/s |
| $K_Q$ | = constant dependent on flight condition |
| $p$ | = roll rate |
| $Q$ | = dynamic pressure |
| $q$ | = pitch rate |
| $r$ | = yaw rate |
| $S$ | = reference area |
| $u$ | = controller input |
| $z$ | = controlled output |
| $\alpha$ | = angle of attack |
| $\beta$ | = angle of sideslip |
| $\delta_c$ | = commanded roll, pitch, or yaw fin deflection |
| $\delta_p$ | = idealized roll control deflection |
| $\delta_{p,q,r}$ | = actual roll, pitch, or yaw fin deflection |
| $\delta_q$ | = idealized pitch control deflection |
| $\delta_r$ | = idealized yaw control deflection |

## I. Introduction

BANK-TO-TURN (BTT) tactical missiles present a particular challenge to autopilot design. BTT maneuvering is characterized by orienting the maximum aerodynamic normal force with the plane of the commanded direction. This is accomplished by rolling and pitching the missile while maintaining (ideally) a zero sideslip angle. By contrast, skid-to-turn (STT) missiles develop a sideslip angle to change attitude, while the roll rate is minimized or left uncontrolled. The advantages of a BTT airframe include increased range, aerodynamic efficiency, and a greater normal acceleration capability in the commanded direction. Especially in the endgame phase of flight, however, BTT missiles may develop a large roll rate and angle of attack. The high roll rates combined with an asymmetrical airframe produce severe kinematic and aerodynamic cross axis coupling in the nonlinear system dynamics. Compared with STT missiles, it is difficult to uncouple the dynamical equations usable for linear classical single-input/single-output (SISO) design techniques. Despite the possible advantages, currently there are no BTT air interceptor missiles in operation.

In Ref. 1, a survey of design methods for BTT autopilots is presented. A classical approach, typified by Ref. 2, initially ignores dynamic coupling by treating each of the pitch, yaw, and roll axes separately. Linearized models are used for each channel, and controllers are designed using SISO frequency response and root locus methods. Then kinematic cross coupling is counteracted by adding cross-coupling paths from the roll channel into the pitch and yaw channels. Modern state-space designs are found in Refs. 3–5. These largely decouple the dynamics by assuming an axisymmetric geometry and simplified aerodynamic modeling. Linear quadratic Gaussian methods are used to design controllers, and the gains are typically scheduled as a function of roll rate and dynamic pressure. Nonlinear simulations are used to verify stability and performance. Both methods achieved comparable performance, but the linear regulator designs resulted in improved robustness properties.

Robust autopilot design has also been investigated in Refs. 6 and 7 using $\mathcal{H}^\infty$ and $\mu$ synthesis, which exploits the structure of the system uncertainties to achieve robust performance. They employ linearized dynamics and uncertainty models, and in Ref. 6 the robust linear time invariant (LTI) controllers are scheduled as a function of angle of attack. Explicitly nonlinear methods to robust autopilot design are found in Refs. 8–10.

A novel approach to gain-scheduled missile autopilot design is presented in Ref. 11. Recall that in a traditional gain-scheduled design, the linear design plants are derived by considering small perturbations about an operating trajectory or flight condition. In Ref. 11, rather than linearizing via a Taylor series truncation, a family of linear plants is derived from a state transformation of the original nonlinear dynamics. Since there is no linearization involved, it is not limited to the local operating point. This method is applied to a longitudinal missile autopilot, in which angle of attack is the scheduling variable. Such families of linear plants indexed by a scheduling variable are referred to as linear parameter varying (LPV). These differ from linear time-varying plants in that the parameter variations are unknown a priori, but may be estimated upon system operation.

References 12–14 focus on theoretical aspects and limitations of gain-scheduled LPV systems. Reference 13 formalizes the notion

Received July 21, 1995; revision received Feb. 12, 1996; accepted for publication March 15, 1996. 

*Graduate Student, Department of Aerospace Engineering and Engineering Mechanics.
†Associate Professor, Department of Aerospace Engineering and Engineering Mechanics. Member AIAA.

that the scheduling variable must vary slowly to maintain stability. Attempts to account for fast parameter variations in the control design are found in Refs. 12 and 14.

This paper closely follows the gain-scheduling approach of Ref. 11, but considers the BTT missile control problem. The goal is to explicitly retain the kinematic and aerodynamic nonlinearities inherent in a BTT airframe, while using design models capable of powerful linear, multivariable, robust design techniques. The missile is considered during the endgame, when a large and rapidly varying angle of attack and roll rate make such nonlinearities the most significant. The main sections of the present approach are summarized as follows. First, LPV systems are defined and are shown to be expressible by certain nonlinear systems. Then the missile mathematical model is developed to include (most) kinematic and inertial coupling. Next the dynamics are brought into LPV form by considering separate pitch and yaw/roll dynamics and applying a suitable transformation. An uncertainty model is developed, and robust controllers are designed at fixed parameter values using $\mu$ synthesis. A global controller is created by switching among the frozen parameter designs dependent on the instantaneous operating point. The closed-loop response to step and pulse commands is simulated with the original nonlinear plant. Finally, robustness to uncertainties not explicitly addressed in the design process is investigated by perturbing coefficients in the aerodynamic model.

## II. Nonlinear Systems as LPV Plants

LPV systems 11–13 are defined as linear systems whose dynamics depend on exogenous time-varying parameters. A state–space description of an LPV system can be represented as

$$\dot{x} = A(\theta)x(t) + B(\theta)u(t) \tag{1}$$

$$y = C(\theta)x(t) \tag{2}$$

where $\theta$ is a vector of parameters unknown a priori but may be estimated on operation of the system. Typically, bounds on the parameter magnitude and rate are known. LPV systems, therefore, differ from LTV systems in that the time variations of the state–space realization matrices in the latter are known beforehand.

A family of controllers $K_\theta$ can be designed at each frozen parameter $\theta$ value, and well-known linear design techniques may be used, utilizing convenient computer-aided design software tools. A gain-scheduling scheme may then consist of interpolating or switching between the linear controllers along the system trajectory.

Although these fixed parameter designs may exhibit good stability and robustness margins for fixed parameter values, fast variations may be destabilizing.[12,13] Therefore, only extensive simulations can verify control system performance for a particular design.

Certain nonlinear systems can also be represented as LPV plants. The nonlinear system is brought into LPV form using a suitable (nonlinear) transformation. In this case the exogenous parameters are actually endogenous to the state dynamics, hence the name quasi-LPV. An example of this was shown in Refs. 11 and 12 for the following nonlinear plant:

$$\frac{\mathrm{d}}{\mathrm{d}t}\begin{pmatrix} z \\ w \end{pmatrix} = f(z) + A(z)\begin{pmatrix} z \\ w \end{pmatrix} + B(z)u \tag{3}$$

References 11 and 12 call these systems output nonlinear since the nonlinearities only depend on the measured output $z$. To transform the system to quasi-LPV form, assume that there exist continuously differentiable functions $w_{eq}(z)$ and $u_{eq}(z)$ such that

$$f(z) + A(z)\begin{bmatrix} z \\ w_{eq}(z) \end{bmatrix} + B(z)u_{eq}(z) = 0 \tag{4}$$

Then $A(z)$ and $B(z)$ are partitioned to conform with $(z\ \ w)^T$ as

$$A(z) = \begin{bmatrix} A_{11}(z) & A_{12}(z) \\ A_{21}(z) & A_{22}(z) \end{bmatrix}, \qquad B(z) = \begin{bmatrix} B_1(z) \\ B_2(z) \end{bmatrix} \tag{5}$$

After some manipulation, the state dynamics can be written as

$$\frac{\mathrm{d}}{\mathrm{d}t}\begin{bmatrix} z \\ w - w_{eq}(z) \end{bmatrix} = \begin{bmatrix} 0 & A_{12}(z) \\ 0 & A_{22}(z) - Dw_{eq}(z)A_{12}(z) \end{bmatrix} \times \begin{bmatrix} z \\ w - w_{eq}(z) \end{bmatrix} + \begin{bmatrix} B_1(z) \\ B_2(z) - Dw_{eq}(z)B_1(z) \end{bmatrix}[u - u_{eq}(z)] \tag{6}$$

where $w - w_{eq}(z)$ is the deviation away from the instantaneous equilibrium state parameterized by the output nonlinearity. The operator $D$ in Eq. (6) represents differentiation with respect to $z$ applied to $w_{eq}(z)$. Equation (6) is a quasi-LPV representation of the original nonlinear plant. Note that the linearization is a result of a state transformation, rather than to a truncated Taylor series expansion about equilibrium values.

Next, integrators are augmented at the plant input to get the final design plant. As shown in Ref. 11, this is desirable to avoid updating the applied control signal by the equilibrium term $u_{eq}(z)$, and also to reduce steady-state tracking errors. Letting

$$u = \int v$$

the state dynamics become

$$\frac{\mathrm{d}}{\mathrm{d}t}\begin{bmatrix} z \\ w - w_{eq}(z) \\ u - u_{eq}(z) \end{bmatrix} = \begin{bmatrix} 0 & A_{12}(z) & B_1(z) \\ 0 & A_{22}(z) - Dw_{eq}(z)A_{12}(z) & B_2(z) - Dw_{eq}(z)B_1(z) \\ 0 & -Du_{eq}(z)A_{12}(z) & -Du_{eq}(z)B_1(z) \end{bmatrix} \times \begin{bmatrix} z \\ w - w_{eq}(z) \\ u - u_{eq}(z) \end{bmatrix} + \begin{bmatrix} 0 \\ 0 \\ 1 \end{bmatrix} v \tag{7}$$

A series of controllers can be designed at fixed $z$ values using the design plant, and a gain-scheduling scheme implemented. Note that although the controllers are linear designs, the control law is nonetheless nonlinear because of the feedback of the $w_{eq}(z)$ and $u_{eq}(z)$ equilibrium conditions. The following sections, in which this framework is applied to a BTT missile autopilot design, illustrate this more clearly.

## III. Missile Dynamics

The differential equations used to describe the missile dynamics were derived in a manner similar to that in Ref. 15. They are representative of a BTT airframe traveling at Mach 2.75 at an altitude of 40,000 ft. The body $x$ axis is oriented longitudinally along the airframe, positive from aft to forward. The body $z$ axis points toward the ground in level flight, and the body $y$ axis completes the right-hand rule. The missile is considered in the endgame phase of flight, and so the total translational velocity magnitude and mass are assumed constant. Furthermore, gravity terms are neglected, but may later be added into the guidance command as a bias. Since a BTT missile is nearly symmetrical in the pitch plane, two of the three cross products of inertia ($I_{xy}$, $I_{yz}$) are assumed to be zero. With these assumptions, the missile dynamics are as follows:

$$\dot{\alpha} = K_Q[-C_x \sin\alpha + C_z \cos\alpha] - \tan\beta(p\cos\alpha + r\sin\alpha) + q \tag{8}$$

$$\dot{\beta} = K_Q[C_y \cos\beta - C_x \cos\alpha \sin\beta - C_z \sin\alpha \sin\beta] - r\cos\alpha - p\sin\alpha \tag{9}$$

$$\dot{p} = I_1 pq + I_2 QSdC_l + I_3 QSdC_n \tag{10}$$

$$\dot{q} = (1/I_{yy})\left[I_{xz}(r^2 - p^2) + (I_{zz} - I_{xx})pr + QSdC_m\right] \tag{11}$$

$$\dot{r} = I_4 pq + I_3 QSdC_l + I_5 QSdC_n \tag{12}$$

The missile mass property and flight condition data are given in the Appendix. Note that the preceding equations exhibit significant explicit kinematic and inertial coupling, and implicit coupling through the aerocoefficients. Specifically, a BTT missile will develop a large roll rate and angle of attack while maintaining a small sideslip angle. Therefore, the roll rate will require a large yaw rate through Eq. (9) to maintain zero sideslip. These roll/yaw rates will then be coupled into the pitch plane dynamics via Eq. (11). The pitch dynamics also appear in the yaw/roll equations.

The controls appear in the aerodynamic force and moment coefficients, which, in general, are complicated nonlinear functions of both the states and the controls. These are in the form of tabular data, and so functional approximations were created by curve fitting. The resulting aerodynamic model is as follows:

$$C_x(\alpha) = C_{x_0} + C_{x_\alpha}\alpha \tag{13}$$

$$C_y(\beta, \delta_r) = C_{y_\beta}\beta + C_{y_{\delta_r}}\delta_r \tag{14}$$

$$C_z(\alpha, \delta_q) = C_{z_0} + C_{z_\alpha}\alpha + C_{z_{\delta_q}}\delta_q \tag{15}$$

$$C_l(\alpha, \beta, \delta_p, \delta_r) = (a_1 + a_2\alpha)\beta + C_{l_{\delta_p}}\delta_p + a_3\alpha\delta_r \tag{16}$$

$$C_m(\alpha, \delta_q) = C_{m_0} + C_{m_\alpha}\alpha + C_{m_{\delta_q}}\delta_q \tag{17}$$

$$C_n(\delta_r) = C_{n_{\delta_r}}\delta_r \tag{18}$$

A real missile airframe produces these idealized control deflections through fin mixing logic, not modeled here. All other terms in Eqs. (13–18) are constant stability derivatives, which are given in the Appendix. These functions were chosen to approximate the tabular data to within ±20% over a range of $\alpha = [-10, 20]$ deg and $\beta = \pm 5$ deg.

The missile tail-fin actuators are modeled as first-order systems as per Ref. 5, with the transfer function

$$\delta_{p,q,r}(s) = [K_a/(s + K_a)]\delta_c(s) \tag{19}$$

Actuator constraints for this BTT airframe are given in Ref. 16 as a 55-deg maximum fin deflection magnitude and a 300-deg/s fin deflection rate.

## IV. Missile Autopilot Design

The following sections present the missile autopilot design. The quasi-LPV method is applied to the BTT missile airframe dynamics to yield a pitch/yaw/roll gain-scheduled controller. The states $(\alpha\ \beta\ p\ q\ r)^T$ are assumed available for feedback, but in practice must be estimated using accelerometer and rate gyro measurements. The robust control design proceeds using $\mu$ synthesis, which is first briefly reviewed in Sec. IV.A. Section IV.B discusses the general design goals and methodology. The control law is designed in two separate channels, referred to as the pitch channel and the yaw/roll channel. These designs are presented in Secs. IV.C and IV.D, respectively.

### A. $\mu$ Synthesis

In this section, we present a very brief overview of $\mu$ synthesis for linear plants. See Ref. 17 for a more detailed discussion.

First, we establish the following notation (see Ref. 18). For a time signal $g$, we define $\|g\|$ as

$$\|g\| \stackrel{\text{def}}{=} \left[\int_0^\infty g^T(t)g(t)\,dt\right]^{\frac{1}{2}} \tag{20}$$

For a stable dynamical system $H$, we define $\|H\|$ as

$$\|H\| \stackrel{\text{def}}{=} \sup_{g\neq 0} \frac{\|Hg\|}{\|g\|} \tag{21}$$

If case $H$ is LTI, then

$$\|H\| = \sup_\omega \sigma_{\max}[H(j\omega)] \tag{22}$$

Figure 1 shows the general structure for $\mu$ synthesis. In this figure, the block $G$ denotes the generalized plant, i.e., the plant to be controlled as well as various weightings/normalizations on the time signals and modeling errors. The block $\Delta$ denotes a block-diagonal system of LTI perturbations, which capture plant uncertainties and express performance objectives. We assume $\Delta$ has been normalized (via weightings absorbed into $G$), so that $\|\Delta\| \leq 1$. The signal $d$ contains all external inputs, $x$ is an error signal, $y$ is the vector of measurements, and $u$ is the control input. Let $T_{dx}(K)$ denote the closed-loop transfer function from $x$ to $d$. It is well known that $\|T_{dx}(K)\|$ is an upper bound for a necessary and sufficiency condition of robust performance for all admissible $\Delta$. In case the perturbations are structured (e.g., $\Delta$ is block diagonal), the upper bound is arbitrarily conservative. Nevertheless, $\|T_{dx}(K)\| < 1$ implies robust performance achieved. A $\mu$-synthesis design exploits the structure of $\Delta$ to produce a controller $K$ that delivers robust performance.

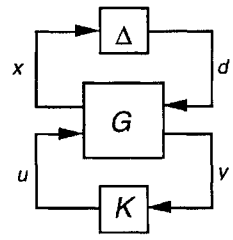


**Fig. 1 Generalized plant interconnection structure.**

The $\mu$-synthesis design procedure is described as follows. The objective is to find a controller $K_*$ and a diagonal scaling $D_*$ such that $\|D_* T_{dx}(K_*) D_*^{-1}\| < 1$. This implies robust performance for all admissible perturbations. The diagonal structure of $D_*$ is set to appropriately match the diagonal structure of $\Delta$ (see Ref. 17).

A design via $\mu$ synthesis seeks to achieve the aforementioned goal by minimizing $\|DT_{dx}(K)D^{-1}\|$ over stabilizing $K$ and appropriate diagonal $D$. This quantity is minimized by alternatively minimizing over $K$ and $D$. First, design a controller $K_0$ such that $\|T_{dx}(K_0)\|$ is minimized. Second, find a diagonal scaling $D_0$ such that $\|D_0 T_{dx}(K_0) D_0^{-1}\|$ is minimized. Next, design a controller $K_1$ such that $\|D_0 T_{dx}(K_1) D_0^{-1}\|$ is minimized. Then, find a diagonal scaling $D_1$ such that $\|D_1 T_{dx}(K_1) D_0^{-1}\|$ is minimized, etc. This process, known as $D$–$K$ iteration, continues as long as each iteration provides a sufficient reduction in the cost function $\|DT_{dx}D^{-1}\|$. Although $D$–$K$ iteration need not find a global minimum, it can often lead to good results.

### B. Design Methodology

The guidance commands for a BTT airframe may require a large angle of attack and roll rate, while minimizing the sideslip angle. When both the angle of attack and roll rate become large, the dynamic cross-coupling nonlinearities become most evident. The closed-loop design goals are, therefore, to follow a simultaneous 20-deg step command in angle of attack $\alpha_c$, and a 500-deg/s roll rate command $p_c$. The sideslip angle $\beta$ is commanded to zero. In practice, $\alpha$ is not commanded directly, but indirectly via normal acceleration commands. The performance specifications are to track the step commands in angle of attack and roll rate with a steady-state accuracy of less than 0.5% and a time constant of 0.2 s, while maintaining $|\beta| \leq 5$ deg. Furthermore, performance must be maintained in the presence of (unmodeled) flexible mode dynamics.

As previously noted, the missile dynamics are highly coupled and nonlinear. A high roll rate and angle of attack induce a high yaw rate and pitch/yaw/roll kinematic coupling. The design challenge is to devise linear design models conducive to gain-scheduling techniques, while capturing the nonlinear structure of the system. The present approach uses the quasi-LPV framework to yield linear design plants not the result of Taylor series truncations. In Ref. 11, this was done for a longitudinal missile autopilot.

Toward this end, we seek a partition of the nonlinear missile dynamics [Eqs. (8–12)], in the form of $[z\ \ w]^T$, such that the dynamics can be written as in Eq. (3). In others words, all nonlinearities must be contained within the $z$ states, or as products with the $w$ states. Then a set of algebraic nonlinear equations must be solved [Eq. (4)] for the equilibrium functions $w_{eq}(z)$ and $u_{eq}(z)$. No such analytical solution can be found for the missile problem, however, without greatly simplifying the dynamics.

To facilitate the transformation into LPV form, the control design is separated into a pitch channel and a yaw/roll channel. That is, the pitch channel uses only the $\dot{\alpha}$ and $\dot{q}$ equations. A pitch control law is designed for the pitch control deflection $\delta_q$ to achieve the commanded angle of attack $\alpha_c$. The yaw/roll states are not regulated, but rather they are considered exogenous varying parameters.

Similarly, the yaw/roll channel uses only the $\dot{\beta}$, $\dot{p}$, and $\dot{r}$ equations. A yaw/roll control law is designed for the yaw control deflection $\delta_r$ and for the roll control deflection $\delta_p$, to achieve the commanded roll rate $p_c$ and zero sideslip. Again, in this case the pitch states are considered exogenous varying parameters.

Another reason for our approach is the physical intuition that the pitch deflection primarily affects the angle of attack and pitch rate, while the yaw/roll deflections primarily affect the sideslip angle, yaw, and roll rates.

### C. Pitch Channel Autopilot

For the purpose of design, the only additional assumption to be made is that the sideslip angle $\beta$ is small. Then the pitch dynamics [Eqs. (8) and (11)] can be written as

$$\begin{pmatrix}\dot{\alpha}\\ \dot{q}\end{pmatrix} = f(\alpha, p, r) + \begin{bmatrix}0 & 1\\ 0 & 0\end{bmatrix}\begin{pmatrix}\alpha\\ q\end{pmatrix} + B(\alpha)\delta_q \tag{23}$$

where

$$f(\alpha, p, r) = \begin{pmatrix} K_Q\left[-\left(C_{x_0} + C_{x_\alpha}\alpha\right)\sin\alpha + \left(C_{z_0} + C_{z_\alpha}\alpha\right)\cos\alpha\right] \\ \left[I_{xz}(r^2 - p^2) + (I_{zz} - I_{xx})pr + QSd\left(C_{m_0} + C_{m_\alpha}\alpha\right)\right]/I_{yy}\end{pmatrix} \tag{24}$$

$$B(\alpha) = \begin{pmatrix} C_{z_{\delta_q}}\cos\alpha \\ QSdC_{m_{\delta_q}}/I_{yy}\end{pmatrix} \tag{25}$$

These equations are in the form of Eq. (3), where $z = \alpha$ and $w = q$. The yaw/roll states $(p, r)$ are considered exogenous parameters. Next, Eq. (4) is solved for the equilibrium functions $u_{eq}(z)$ and $w_{eq}(z)$, resulting in

$$u_{eq}(z) = \delta_{q_{eq}}(\alpha, p, r) = \frac{-(C_{m_0} + C_{m_\alpha}\alpha)}{C_{m_{\delta_q}}} + \frac{I_{xz}(r^2 - p^2) + (I_{zz} - I_{xx})pr}{QSdC_{m_{\delta_q}}} \tag{26}$$

$$w_{eq}(z) = q_{eq}(\alpha, p, r) = -K_Q\left[-\left(C_{x_0} + C_{x_\alpha}\alpha\right)\sin\alpha + \left(C_{z_0} + C_{z_\alpha}\alpha + C_{z_{\delta_q}}\delta_{q_{eq}}\right)\cos\alpha\right] \tag{27}$$

Thus, the pitch dynamics can be written in the form of Eq. (7), leading to the pitch channel state space

$$\frac{\mathrm{d}}{\mathrm{d}t}\begin{bmatrix}\alpha\\ q - q_{eq}\\ \delta_q - \delta_{q_{eq}}\end{bmatrix} = A_p(\alpha, p, r)\begin{bmatrix}\alpha\\ q - q_{eq}\\ \delta_q - \delta_{q_{eq}}\end{bmatrix} + \begin{bmatrix}0\\ 0\\ 1\end{bmatrix}\nu \tag{28}$$

Lastly, the actuator dynamics are augmented, which results in the final pitch channel design plant

$$\frac{\mathrm{d}}{\mathrm{d}t}\begin{bmatrix}\alpha\\ q - q_{eq}\\ \delta_q - \delta_{q_{eq}}\\ x_a\end{bmatrix} + \begin{bmatrix}A_p(\alpha, p, r) & \begin{pmatrix}0\\0\\1\end{pmatrix}\\ (0\ \ 0\ \ 0) & -K_a\end{bmatrix} \times \begin{bmatrix}\alpha\\ q - q_{eq}\\ \delta_q - \delta_{q_{eq}}\\ x_a\end{bmatrix} + \begin{bmatrix}0\\0\\0\\K_a\end{bmatrix}\delta_c \tag{29}$$

where $x_a$ is the actuator state variable.

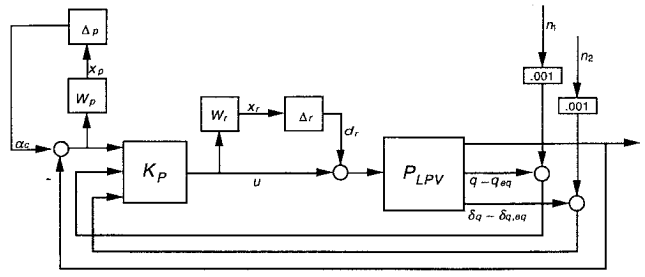


**Fig. 2 Pitch channel interconnection structure.**

Using the plant family, robust controllers are designed via $\mu$ synthesis at fixed $(\alpha, p, r)$ values. To facilitate this, we seek to connect the design plant to weighted perturbation blocks that represent the performance and robustness objectives, as shown in Fig. 1.

The resulting interconnection structure for the pitch channel analogous to Fig. 1 is shown in Fig. 2, where

$$\boldsymbol{d} = \begin{pmatrix}\alpha_c\\ d_r\\ n_1\\ n_2\end{pmatrix} \tag{30}$$

$$\boldsymbol{x} = \begin{pmatrix}x_p\\ x_r\\ x_p\end{pmatrix} \tag{31}$$

$$\boldsymbol{y} = \begin{pmatrix}\alpha_c - \alpha\\ q - q_{eq} + n_1\\ \delta_q - \delta_{q_{eq}} + n_2\end{pmatrix} \tag{32}$$

The components of vector $\boldsymbol{d}$ are all of the external inputs to the generalized plant including disturbances and commands. The components of $\boldsymbol{x}$ are the (weighted) error outputs of the generalized plant. Specifically, the perturbation block $\Delta_p$ is an artificial uncertainty placed noting that minimizing the dynamics from $\alpha_c$ to $x_p$ is equivalent to achieving good tracking performance. The uncertainty block $\Delta_r$ reflects unmodeled flexible mode dynamics, and so minimizing the transfer function from $d_r$ to $x_r$ implies robust stability to all admissible $\Delta_r$. Norm minimization with respect to the (block diagonal) structured uncertainty composed of both $\Delta_p$ and $\Delta_r$ implies robust performance.

The signals $n_1$ and $n_2$ are small artificial noise inputs augmented to $\boldsymbol{d}$ to satisfy certain rank conditions in the generalized plant, as required by the $\mu$-synthesis procedure. The signal $x_p$ is augmented to the bottom of the error vector to improve the numerical conditioning of the design algorithm by reflecting the effects of $n_1$ and $n_2$ on tracking error. The measured plant output is $\boldsymbol{y}$, and the control $u$ equals $\delta_c$ in Eq. (29).

The $W_r$ and $W_p$ blocks are the robustness and performance weighting functions, respectively. A representative flexible mode transfer function from tail deflection to rate-sensor measurement for a BTT airframe is given in Ref. 6. The function $W_r(s)$ is therefore chosen to be a frequency-dependent magnitude bound on the unmodeled transfer function. Figure 3 shows $W_r(s)$, where

$$W_r(s) = 100\frac{(s + 100)(s + 200)}{(s + 10000)(s + 20000)} \tag{33}$$

$W_p$, taken directly from Ref. 6, is shown in Fig. 4 and given by

$$W_p(s) = \frac{(14.9451s + 200)}{(42.7003s + 1)} \tag{34}$$

Six pitch channel controllers were designed at the following set points of $\alpha$ and $p$. The design yaw rate $r$ in each case was set to

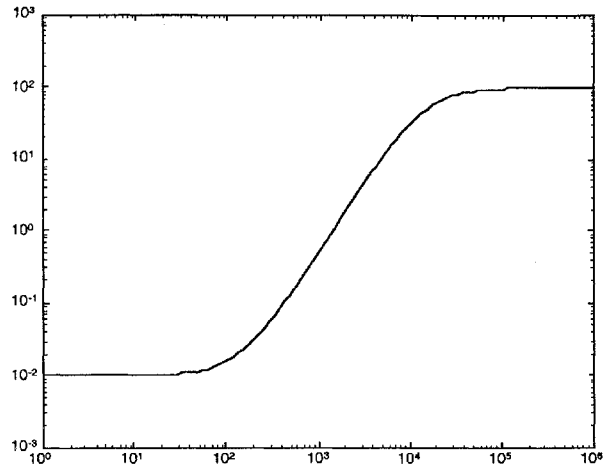

**Fig. 3 Robustness weight $W_r(j\omega)$.**

approximate the steady-state value $r_{ss} = -p \tan\alpha$. The units are in degree and degree per second:

$K_{P11}$, for $\alpha = 0$, $p = 0$ $\quad$ $K_{P12}$, for $\alpha = 0$, $p = 300$

$K_{P21}$, for $\alpha = 20$, $p = 0$ $\quad$ $K_{P22}$, for $\alpha = 20$, $p = 300$

$K_{P13}$, for $\alpha = 0$, $p = 500$ $\quad$ $K_{P23}$, for $\alpha = 20$, $p = 500$

After three $D$–$K$ iterations, each of the six controllers were reduced from an initial cost function of $\|T_{dx}(K)\| = 2$ to a final value of 1.06. This implies robust performance is achieved for all LTI stable $\|\Delta\| \leq 1/1.06 = 0.94$. Since the robustness weighting function is a conservative and approximate bound on the flexible mode dynamics frequency response, the controller is considered adequate.

### D. Yaw/Roll Channel Autopilot

The yaw/roll channel autopilot is developed in a manner very similar to that of the pitch channel. For the design plant, the sideslip angle $\beta$ is again assumed to be small. Then the yaw/roll dynamics [Eqs. (9), (10), and (12)] may be written as

$$\begin{pmatrix} \dot\beta \\ \dot p \\ \dot r \end{pmatrix} = f(\beta, p, \alpha, q) + \begin{bmatrix} K_Q C_{y_\beta} & 0 & -\cos\alpha \\ 0 & 0 & 0 \\ 0 & 0 & 0 \end{bmatrix} \times \begin{pmatrix} \beta \\ p \\ r \end{pmatrix} + B(\alpha) \begin{pmatrix} \delta_p \\ \delta_r \end{pmatrix} \tag{35}$$

where

$$f(\beta, p, \alpha, q) = \begin{pmatrix} -p \sin\alpha \\ I_1 pq \\ I_4 pq \end{pmatrix} \tag{36}$$

$$B(\alpha) = \begin{pmatrix} 0 & C_{y_{\delta_r}} \\ I_2 QSdC_{l_{\delta_p}} & QSd\left(I_2 a_3 \alpha + I_3 C_{n_{\delta_r}}\right) \\ I_3 QSdC_{l_{\delta_p}} & QSd\left(I_3 a_3 \alpha + I_5 C_{n_{\delta_r}}\right) \end{pmatrix} \tag{37}$$

Again, these equations are in the form of Eq. (3), where $z = [\beta \;\; p]^T$ and $w = r$. The pitch states $(\alpha, q)$ are treated as exogenous parameters. Equation (4) is again solved for the equilibrium functions $u_{eq}(z)$ and $w_{eq}(z)$, where $u_{eq}(z)$ contains two components corresponding to the roll control deflection and the yaw control deflection. The result is

$$u_{eq,1}(z) = \delta_{p_{eq}}(\beta, p, \alpha, q) = \frac{-\left(I_3 a_3 \alpha + I_5 C_{n_{\delta_r}}\right)\delta_{r_{eq}}}{I_3 C_{l_{\delta_p}}} - \frac{I_4 pq}{I_3 QSdC_{l_{\delta_p}}} \tag{38}$$

$$u_{eq,2}(z) = \delta_{r_{eq}}(\beta, p, \alpha, q) = \frac{pq(I_2 I_4 - I_1 I_3)}{QSdC_{n_{\delta_r}}\left(I_3^2 - I_2 I_5\right)} \tag{39}$$

$$w_{eq}(z) = r_{eq}(\beta, p, \alpha, q) = \frac{K_Q\left[C_{y_\beta}\beta + C_{y_{\delta_r}}\delta_{r_{eq}}\right]}{\cos\alpha} - p\tan\alpha \tag{40}$$

The yaw/roll dynamics can be written in the form of Eq. (7), leading to the yaw/roll channel state space

$$\frac{\mathrm{d}}{\mathrm{d}t}\begin{bmatrix} \beta \\ p \\ r - r_{eq} \\ \delta_p - \delta_{p_{eq}} \\ \delta_r - \delta_{r_{eq}} \end{bmatrix} = A_y(\beta, p, \alpha, q) \begin{bmatrix} \beta \\ p \\ r - r_{eq} \\ \delta_p - \delta_{p_{eq}} \\ \delta_r - \delta_{r_{eq}} \end{bmatrix} + \begin{bmatrix} 0 & 0 \\ 0 & 0 \\ 0 & 0 \\ 1 & 0 \\ 0 & 1 \end{bmatrix} \begin{bmatrix} \nu_1 \\ \nu_2 \end{bmatrix} \tag{41}$$

With augmented actuator dynamics, the yaw/roll design plant becomes

$$\frac{\mathrm{d}}{\mathrm{d}t}\begin{bmatrix} \beta \\ p \\ r - r_{eq} \\ \delta_p - \delta_{p_{eq}} \\ \delta_r - \delta_{r_{eq}} \\ x_{1a} \\ x_{2a} \end{bmatrix} = \begin{bmatrix} A_y(\beta, p, \alpha, q) & \begin{pmatrix} 0 & 0 \\ 0 & 0 \\ 0 & 0 \\ 1 & 0 \\ 0 & 1 \end{pmatrix} \\ \begin{pmatrix} 0 & 0 & 0 & 0 & 0 \\ 0 & 0 & 0 & 0 & 0 \end{pmatrix} & \begin{pmatrix} -K_a & 0 \\ 0 & -K_a \end{pmatrix} \end{bmatrix} \times \begin{bmatrix} \beta \\ p \\ r - r_{eq} \\ \delta_p - \delta_{p_{eq}} \\ \delta_r - \delta_{r_{eq}} \\ x_{1a} \\ x_{2a} \end{bmatrix} + \begin{bmatrix} 0 & 0 \\ 0 & 0 \\ 0 & 0 \\ 0 & 0 \\ 0 & 0 \\ K_a & 0 \\ 0 & K_a \end{bmatrix} \begin{bmatrix} \delta_{c,p} \\ \delta_{c,r} \end{bmatrix} \tag{42}$$

where $x_{1a}$ and $x_{2a}$ are the actuator state variables.

As in the pitch channel, $\mu$ synthesis is performed at fixed $(\alpha, p)$ values. The interconnection structure for the yaw/roll channel is shown in Fig. 5, where

$$\boldsymbol{d} = \begin{pmatrix} \beta_c \\ p_c \\ \boldsymbol{d_r} \\ n_1 \\ n_2 \\ n_3 \end{pmatrix} \tag{43}$$

$$\boldsymbol{x} = \begin{pmatrix} \boldsymbol{x_p} \\ \boldsymbol{x_r} \\ \boldsymbol{x_p} \end{pmatrix} \tag{44}$$

$$\boldsymbol{y} = \begin{pmatrix} \beta_c - \beta \\ p_c - p \\ r - r_{eq} + n_1 \\ \delta_p - \delta_{p_{eq}} + n_2 \\ \delta_r - \delta_{r_{eq}} + n_3 \end{pmatrix} \tag{45}$$

In this case the signals represented by the boldface variables $(\boldsymbol{d_r}, \boldsymbol{x_p}, \boldsymbol{x_r})$ are two-dimensional vectors. The $W_r$ weighting function is the same as in the pitch channel, except that it is a diagonal $2 \times 2$ block. The performance weighting is also a diagonal $2 \times 2$ block, where each component is given by

$$W_p(s) = \frac{(7s + 200)}{(10s + 1)} \tag{46}$$

Figure 6 shows the frequency response for $W_p(s)$.

Six yaw/roll channel controllers were designed at the following set points of $\alpha$ and $p$, where the sideslip angle and pitch rate were set equal to the corresponding equilibrium values of $\beta = 0$ and $q_{eq}$ given

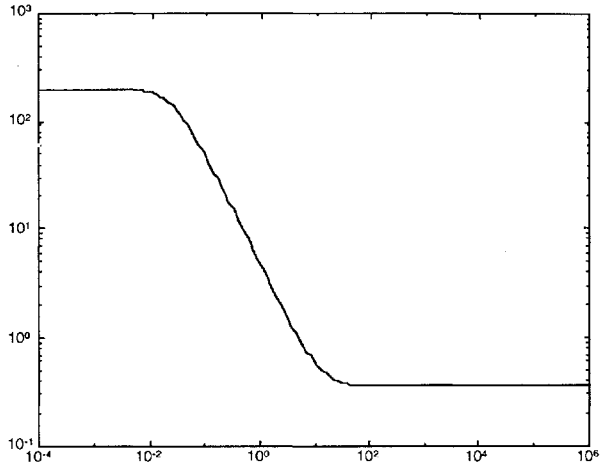

Fig. 4 Performance weight $W_p(j\omega)$ for pitch control.

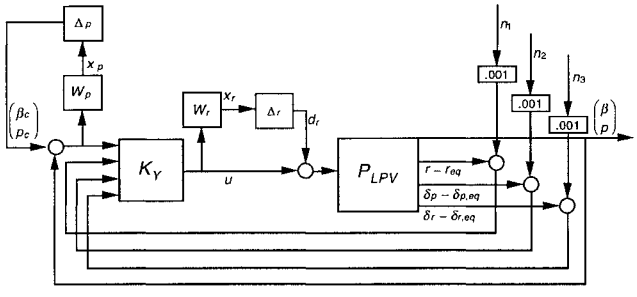


Fig. 5 Yaw/roll channel interconnection structure.

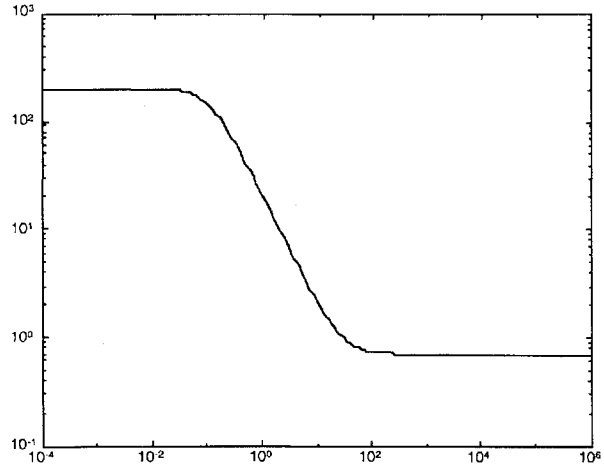

Fig. 6 Performance weight $W_p(j\omega)$ for yaw/roll control.

by Eq. (27). The design yaw rate was again set to $r_{ss} = -p\tan\alpha$. The units are in degree and degree per second:

$K_{Y11}$, for $\alpha = 0$, $p = 0$ $\quad$ $K_{Y12}$, for $\alpha = 0$, $p = 300$

$K_{Y21}$, for $\alpha = 20$, $p = 0$ $\quad$ $K_{Y22}$, for $\alpha = 20$, $p = 300$

$K_{Y13}$, for $\alpha = 0$, $p = 500$ $\quad$ $K_{Y23}$, for $\alpha = 20$, $p = 500$

Again three $D$–$K$ iterations were performed, such that the initial cost function of $\|T_{dx}(K)\| = 2$ was reduced to 1.1. This implies robust performance is achieved for all LTI stable $\|\Delta\| \leq 0.91$. Since the first yaw plane bending and roll plane torsional flexible modes will be at an even higher frequency than the first pitch plane mode, the robustness bound is conservative. Therefore, no further $D$–$K$ iterations are deemed necessary.

## V. Simulation Results

Although the controllers achieved robust performance for fixed parameter values, there is no guarantee of even stability for fast

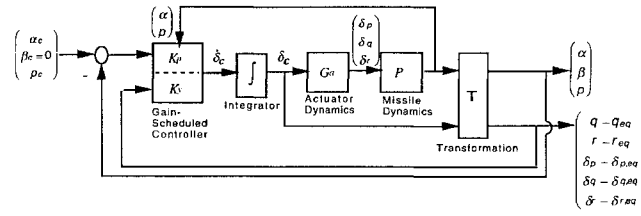


Fig. 7 Implementation of controller.

parameter variations. This is not a result of poor stability margins in the fixed-point designs, but of the true dynamics no longer being accurately represented for fast parameter variations. Furthermore, the controller feeds back updated equilibrium functions of the states, which is a kind of feedback linearization. Simulations with the nonlinear plant are, therefore, required to verify stability and performance.

Figure 7 shows the actual implementation of the pitch/yaw/roll global controller with the nonlinear missile model. The block $T$ represents the transformation to the quasi-LPV form of the state variables. That is, the missile states are transformed to the alternate state description given by Eq. (7) for a general system. For our missile problem, this necessitates calculation of equilibrium functions given by Eqs. (26) and (27) for the pitch channel and Eqs. (38–40) for the yaw/roll channel.

From Eqs. (29) and (42) we can see that the actual fin deflections ($\delta_p$, $\delta_q$, $\delta_r$) are required. These are assumed to be unknown due to actuator dynamics, and so the commanded fin deflections are used for feedback. Note that although the control designs were linear, the control law is nonlinear because of the transformation (and the gain scheduling).

The previous control design resulted in six linear dynamic controllers each for the pitch and yaw/roll channels. The pitch controller uses as input the states $(\alpha \;\; q - q_{\text{eq}} \;\; \delta_{q,c} - \delta_{q,\text{eq}})^T$ to produce the derivative of the commanded pitch fin deflection $\dot{\delta}_{q,c}$. The yaw/roll channel inputs the states $(\beta \;\; p \;\; r - r_{\text{eq}} \;\; \delta_{p,c} - \delta_{p,\text{eq}} \;\; \delta_{r,c} - \delta_{r,\text{eq}})^T$ to produce the derivative of the commanded roll and yaw fin deflections, $\dot{\delta}_{p,c}$ and $\dot{\delta}_{r,c}$. At any given moment in time, one of the six controllers for each channel is chosen, dependent on the instantaneous values of $\alpha$ (deg) and $p$ (deg/s) as follows:

$$K_{P,Y} = \begin{cases} K_{11} & \text{for} \quad \alpha \leq 10 \quad p \leq 150 \\ K_{12} & \text{for} \quad \alpha \leq 10 \quad 150 < p \leq 400 \\ K_{21} & \text{for} \quad \alpha > 10 \quad p \leq 150 \\ K_{22} & \text{for} \quad \alpha > 10 \quad 150 < p \leq 400 \\ K_{13} & \text{for} \quad \alpha \leq 10 \quad p > 400 \\ K_{23} & \text{for} \quad \alpha > 10 \quad p > 400 \end{cases} \tag{47}$$

The control gains are switched along the missile trajectory according to the preceding schedule.

The pitch equilibrium functions $\delta_{q\text{eq}}(\alpha, p, r)$ and $q_{\text{eq}}(\alpha, p, r)$ are updated continuously with the current value of $\alpha$, and switched with the design values of $(p, r)$ according to the schedule. The yaw/roll equilibrium functions $\delta_{p\text{eq}}(\beta, p, \alpha, q)$, $\delta_{r\text{eq}}(\beta, p, \alpha, q)$, and $r_{\text{eq}}(\beta, p, \alpha, q)$ are updated continuously with current values of all independent variables.

The missile was trimmed at $\alpha = 0$ deg and $p = 0$ deg/s, and the response was first simulated to a simultaneous step command of $\alpha = 20$ deg and $p = 500$ deg/s. Figures 8–10 show the resulting step response for the angle of attack, sideslip, and roll rate. Figure 11 shows the pitch, yaw, and roll control deflections. Note that the time domain performance specifications are met, and the fin deflection magnitudes are within the 55-deg constraint. However, the 300-deg/s actuator rate limit is exceeded for the pitch control deflection.

Typically, angle of attack and roll rate are not commanded directly; rather, they are commanded indirectly through acceleration and roll angle commands. In Ref. 11, an acceleration command and feedback outer loop was augmented to the inner-loop angle-of-attack control. This was shown to suppress excessive fin deflections by discouraging drastic angle-of-attack commands such as a large step, even if the outer-loop acceleration command is a step. Indeed, higher-fidelity simulations have shown that a smooth pulse in angle-of-attack response is typical in an endgame maneuver. For example,

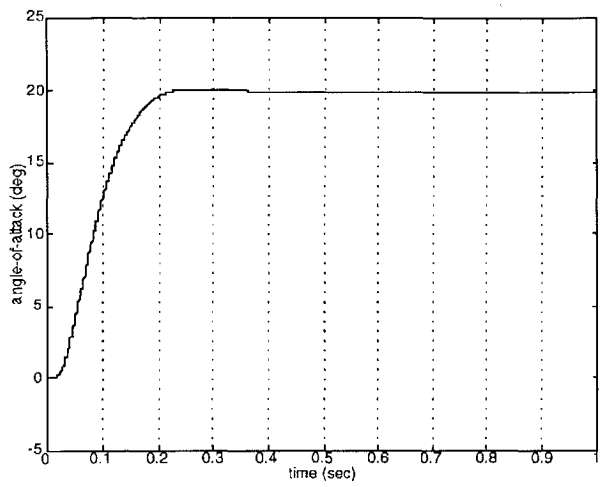


Fig. 8 Angle-of-attack response to step command.

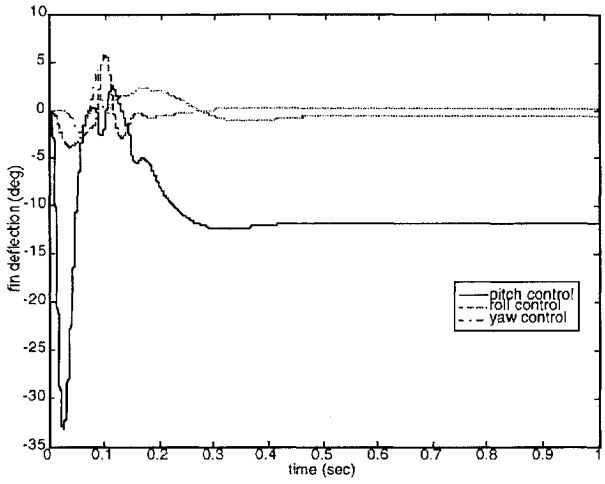


Fig. 11 Control deflections response to step command.

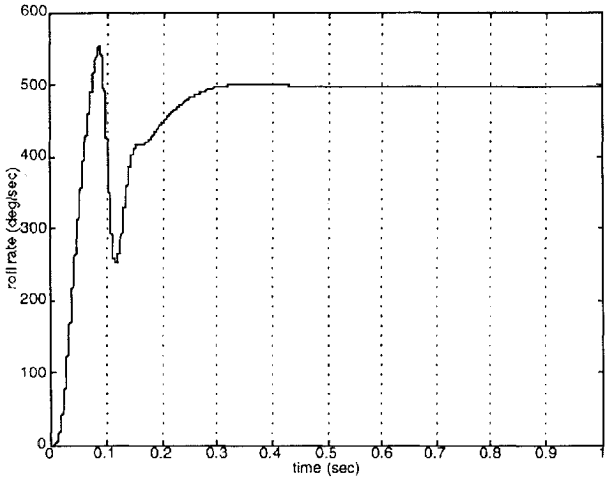


Fig. 9 Roll rate response to step command.

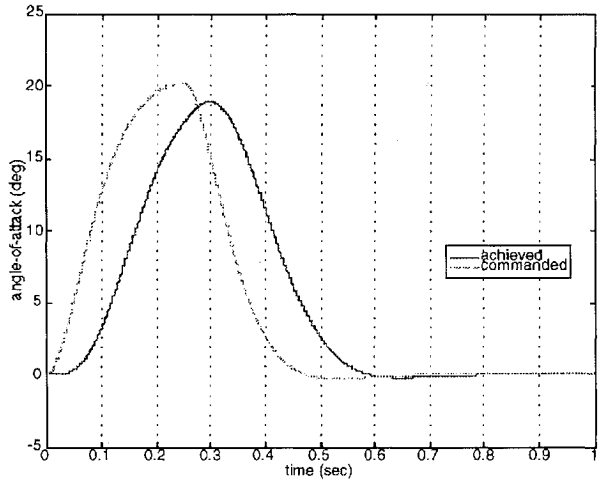


Fig. 12 Angle-of-attack response to pulse command.

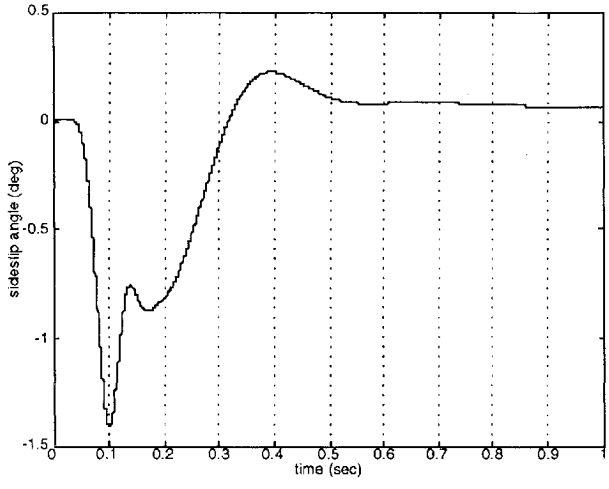


Fig. 10 Sideslip angle response to step command.

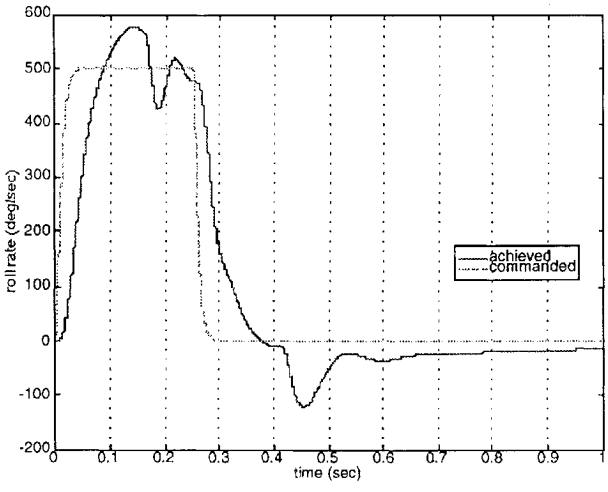


Fig. 13 Roll rate response to pulse command.

in Ref. 3 a BTT missile autopilot is assessed with an accurate six-degree-of-freedom simulation. The simulation includes both a target dynamics model and an acceleration guidance law during the end game. The results show a smooth pulse response of about 18-deg magnitude in angle of attack. See Ref. 3 for more details.

To simulate our missile autopilot under a more realistic endgame scenario, an angle-of-attack command was created by passing a 20-deg magnitude square pulse through a second-order integrator. The result is a smooth pulse angle-of-attack command approximate in frequency and magnitude to that in Ref. 3. To be conservative, the missile was also given a simultaneous 500-deg/s square pulse roll rate command. This type of roll rate command is consistent with that implied by the roll angle error response shown in Ref. 3. Figures 12 and 13 show the time response for the commanded and achieved angle of attack and roll rate. Figure 14 shows the control deflections, which are within the given actuator constraints. The sideslip angle, not shown, was well within the 5-deg magnitude bound. Actuator constraints may be addressed in the design process by appropriate changes in the robustness and performance weighting functions.

The robustness to other perturbations not explicitly addressed in the design was investigated by arbitrarily changing certain coefficients in the aerodynamic model simultaneously by $\pm 20\%$. The resulting performance to step commands was negligibly affected.

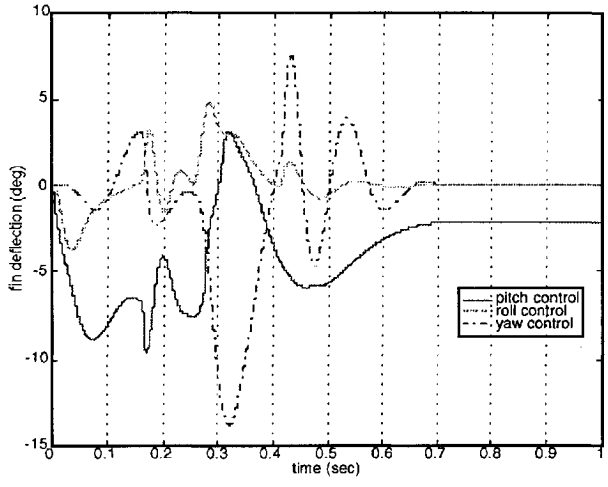


**Fig. 14 Control deflections response to pulse command.**

## VI. Conclusion

This paper presented a gain-scheduled autopilot design for a BTT missile. The missile dynamics are brought into LPV form via a state transformation rather than a local linearization. The coupled, nonlinear dynamics necessitates the use of separate pitch and yaw/roll channels, where the cross channel states are treated as exogenous parameters. Controllers were designed at fixed points using $\mu$ synthesis, and a switching gain scheduler was simulated with the nonlinear missile model using step and pulse commands in angle of attack and roll rate.

Two significant limitations to gain scheduling are linearization assumptions and fast parameter variations. The method presented here addresses the former. Especially for a BTT missile airframe, traditional linearizations may oversimplify system dynamics. We have shown how, by expressing nonlinear systems as quasi-LPV, gain-scheduled design using linear models may proceed without such limitations.

## Appendix: Missile Data

**Flight Condition**

$$\text{Mach} = 2.75, \qquad \text{altitude} = 40{,}000\ \text{ft}$$

$$Q = 2073.7\ \text{lb/ft}^2, \qquad K_Q = 0.0339\ \text{s}^{-1}$$

**Missile Mass Properties and Geometry**

All mass moment of inertias are in slug square foot.

$$I_{xx} = 1.0798, \qquad I_{yy} = 70.131$$

$$I_{zz} = 70.6609, \qquad I_{xz} = -0.7043$$

$$I_1 = \frac{I_{zz}I_{xz} + I_{xz}(I_{xx} - I_{yy})}{I_{xx}I_{zz} - I_{xz}^2} \qquad \text{(dimensionless)}$$

$$I_2 = \frac{I_{zz}}{I_{xx}I_{zz} - I_{xz}^2} \qquad (\text{slug-ft}^2)^{-1}$$

$$I_3 = \frac{I_{xz}}{I_{xx}I_{zz} - I_{xz}^2} \qquad (\text{slug-ft}^2)^{-1}$$

$$I_4 = \frac{I_{xz}^2 + I_{xx}(I_{xx} - I_{yy})}{I_{xx}I_{zz} - I_{xx}^2} \qquad \text{(dimensionless)}$$

$$I_5 = \frac{I_{xx}}{I_{xx}I_{zz} - I_{xx}^2} \qquad (\text{slug-ft}^2)^{-1}$$

$$\text{Weight} = 227\ \text{lb}, \qquad S = 0.3068\ \text{ft}^2, \qquad d = 7.5\ \text{in.}$$

**Aerodynamic Model Coefficients**

$$C_{x_0} = -0.4962, \qquad C_{x_\alpha} = 0.1699$$

$$C_{y_\beta} = -11.1180, \qquad C_{y_{\delta_r}} = 4.6346$$

$$C_{z_0} = -0.1006, \qquad C_{z_\alpha} = -27.2417, \qquad C_{z_{\delta_q}} = -5.4832$$

$$a_1 = 1.4008, \qquad a_2 = -25.7771, \qquad a_3 = -4.4423$$

$$C_{l_{\delta_p}} = -7.2605$$

$$C_{m_0} = -1.4785, \qquad C_{m_\alpha} = -5.6355, \qquad C_{m_{\delta_q}} = -38.7896$$

$$C_{n_{\delta_r}} = -33.6611$$

## Acknowledgments

This research was supported by a U.S. Air Force Office of Scientific Research Summer Graduate Student Fellowship at the U.S. Air Force Armament Directorate, Eglin Air Force Base, FL, and National Science Foundation Grant ECS-9258005. The authors thank Jim Cloutier, Chris D'Souza, and Darren Schumacher for invaluable technical support and guidance. The authors also thank Kristen Kichline for generating the figures and editing.

## References

[1]Cloutier, J. R., Evers, J. H., and Feeley, J. J., "An Assessment of Air-to-Air Missile Guidance and Control Technology," *Proceedings of the American Control Conference*, Inst. of Electrical and Electronics Engineers, Piscataway, NJ, 1988, pp. 133–140.

[2]Kovach, M. J., Stevens, T. R., and Arrow, A., "A Bank-to-Turn Autopilot Design for an Advanced Air-to-Air Interceptor," *Proceedings of the AIAA Guidance, Navigation, and Control Conference* (Monterey CA), AIAA, New York, 1987, pp. 1346–1353.

[3]Williams, D. E., Friedland, B., and Madiwale, A. N., "Modern Control Theory Design of Autopilots for Bank-to-Turn Missiles," *Journal of Guidance, Control, and Dynamics*, Vol. 10, No. 4, 1987, pp. 378–386.

[4]Sheperd, C. L., and Valavani, L., "Autopilot Design for Bank-to-Turn Missiles Using LQG/LTR Methodology," *Proceedings of the American Control Conference*, Inst. of Electrical and Electronics Engineers, Piscataway, NJ, 1988, pp. 579–586.

[5]Bossi, J. A., and Langehough, M. A., "Multivariable Autopilot Designs for a Bank-to-Turn Missile," *Proceedings of the American Control Conference*, Inst. of Electrical and Electronics Engineers, Piscataway, NJ, 1988, pp. 567–572.

[6]Reichert, R. T., "Multivariable Autopilot Designs for a Bank-to-Turn Missile," *Proceedings of the American Control Conference*, Inst. of Electrical and Electronics Engineers, Piscataway, NJ, 1988, pp. 2368–2373.

[7]Lin, C. F., Cloutier, J. R., and Evers, J. H., "High-Performance, Robust, Bank-to-Turn Missile Autopilot Design," *Journal of Guidance, Control, and Dynamics*, Vol. 18, No. 1, 1995, pp. 46–53.

[8]Nichols, R. A., Reichert, R. T., and Rugh, W. J., "Gain Scheduling for $\mathcal{H}^\infty$ Controllers: A Flight Control Example," *IEEE Transactions on Control Systems Technology*, Vol. 1, No. 2, 1993, pp. 69–79.

[9]Adams, R. J., and Banda, S. S., "Robust Flight Control Design Using Dynamic Inversion and Structured Singular Value Synthesis," *IEEE Transactions on Control Systems Technology*, Vol. 1, No. 2, 1993, pp. 80–92.

[10]Hull, R. A., Schumacher, D. A., and Qu, Z., "Design and Evaluation of Robust Nonlinear Missile Autopilots from a Performance Perspective," *Proceedings of the American Control Conference*, Inst. of Electrical and Electronics Engineers, Piscataway, NJ, 1995.

[11]Shamma, J. S., and Cloutier, J. R., "Gain-Scheduled Autopilot Design Using Linear Parameter Varying Transformations," *Journal of Guidance, Control, and Dynamics*, Vol. 16, No. 2, 1993, pp. 256–263.

[12]Shamma, J. S., and Athans, M., "Gain Scheduling: Potential Hazards and Possible Remedies," *IEEE Control Systems Magazine*, Vol. 12, No. 3, 1992, pp. 101–107.

[13]Shamma, J. S., and Athans, M., "Guaranteed Properties of Gain Scheduled Control for Linear Parameter-Varying Plants," *Automatica*, Vol. 27, No. 3, 1991, pp. 559–564.

[14]Apkarian, P., Biannic, J.-M., and Gahinet, P., "Self-Scheduled $\mathcal{H}^\infty$ Control of Missile via Linear Matrix Inequalities," *Journal of Guidance, Control, and Dynamics*, Vol. 18, No. 3, 1995, pp. 532–538.

[15]D'Souza, C. N., and Schumacher, D. A., "Derivation of the Full Nonlinear Equations of Motion for a Rigid Airframe," *Journal of Guidance, Control, and Dynamics* (to be published).

[16]Arrow, A., and Williams, D. E., "Comparison of Classical and Modern Design and Analysis Techniques for a Tactical Air-to-Air Bank-to-Turn Missile," *Proceedings of the Guidance, Navigation, and Control Conference*, Vol. 2, AIAA, New York, 1987, pp. 1360–1371.

[17]Balas, G., Doyle, J. C., Glover, K., Packard, A., and Smith, R., "$\mu$-Analysis and Synthesis Toolbox: $\mu$-Tools," MUSYN, Inc., Minneapolis, MN, and The Mathworks, Inc., Natick, MA, Dec. 1990.

[18]Desoer, C. A., and Vidyasagar, M., *Feedback Systems: Input-Output Properties*, Academic, New York, 1975.